A new multi-component heterogeneous ice nucleation model and its application to Snomax bacterial particles and a Snomax-illte mineral particle mixture

Hassan Beydoun[1], Michael Polen[1], and Ryan C. Sullivan[1,*]

[1]Center for Atmospheric Particle Studies, Carnegie Mellon University, Pittsburgh, PA, USA

*Corresponding author: Ryan C. Sullivan (rsullivan@cmu.edu)

Abstract

Some biological particles, such as Snomax, are very active ice nucleating particles, inducing heterogeneous freezing in supercooled water at temperatures above -15 °C and up to -2 °C. Despite their exceptional freezing abilities, large uncertainties remain regarding the atmospheric abundance of biological ice nucleating particles, and their contribution to atmospheric ice nucleation. It has been suggested that small biological ice nucleating macromolecules or fragments can be carried on the surfaces of dust and other atmospheric particles. This could combine the atmospheric abundance of dust particles with the ice nucleating strength of biological material to create strongly enhanced and abundant ice nucleating surfaces in the atmosphere, with significant implications for the budget and distribution of atmospheric ice nucleating particles, and their consequent effects on cloud microphysics and mixed-phase clouds.

The new critical surface area "$\bar{g}$" framework that was developed by Beydoun et al. (2016), is extended to produce a heterogeneous ice nucleation mixing model that can predict the freezing behavior of multi-component particle surfaces immersed in droplets. The model successfully predicts the immersion freezing properties of droplets containing Snomax bacterial particles across a mass concentration range of seven orders of magnitude, by treating Snomax as comprised of two distinct distributions of heterogeneous ice nucleating activity. Furthermore, the model successfully predicts the immersion freezing behavior of a low concentration mixture of Snomax and illite mineral particles, a proxy for the biological-dust mixtures

observed in atmospheric aerosols. It is shown that even at very low Snomax concentrations in the mixture, droplet freezing at higher temperatures is still determined solely by the second less active and more abundant distribution of heterogeneous ice nucleating activity of Snomax, while freezing at lower temperatures is determined solely by the heterogeneous ice nucleating activity of pure illite. This demonstrates that in this proxy system, biological ice nucleating particles do not compromise their ice nucleating activity upon mixing with dust and no new range of intermediary freezing temperatures associated with the mixture of ice nucleating particles of differing activities is produced. The study is the first to directly examine the freezing behavior of a mixture of Snomax and illite and presents the first multi-component ice nucleation model experimentally evaluated using a wide range of ice nucleating particle concentration mixtures in droplets.

1 Introduction

The potential role certain ice nucleating biological particles may play in cloud physics, meteorology, and global climate has been an active area of research for decades (Ariya et al., 2009; DeMott and Prenni, 2010; Franc and Demott, 1998; Möhler et al., 2007; Morris et al., 2004; Schnell and Vali, 1976). Biological particles such as *Pseudomonas syringae* bacteria can induce freezing in supercooled water at temperatures as high as -2 °C (Hartmann et al., 2012; Polen et al., 2016; Wex et al., 2015). While mineral dust particles are the leading candidate for the most abundant ice nucleating particles (INPs) in the atmosphere (Hoose et al., 2008; Murray et al., 2012), lidar and radar measurements (Bühl et al., 2013) as well as laboratory studies in which melted precipitation samples were refrozen (Christner et al., 2008; Petters and Wright, 2015; Vali, 1971, 1996) have shown that freezing can occur at temperatures higher than -12 °C. This is a temperature range no investigated mineral samples of atmospherically relevant particle sizes (or other atmospherically relevant non-biological particles) have exhibited detectable ice nucleating activity in (Atkinson et al., 2013; Cantrell and Heymsfield, 2005; DeMott et al., 2015; Murray et al., 2012). Furthermore, *in situ* chemical analysis of supercooled cloud drops and ice crystal residues found biological particle material contained within

(Creamean et al., 2013; Kamphus et al., 2010; Pratt et al., 2009). All this evidence points to a potentially important role of biological particles in atmospheric ice nucleation, however significant constraints are still needed to properly account for its contribution to the total atmospheric INP burden and distribution (Möhler et al., 2007).

Schnell and Vali (1976) hypothesized that mineral dust particles can act as inert carriers of biological INPs. Their hypothesis keeps gaining support with early and more recent findings suggesting that biological particles release small ice nucleating macromolecules or fragments (Fröhlich-Nowoisky et al., 2015; Hiranuma et al., 2015b; Wolber et al., 1986) that can be easily lofted and transported on mineral dust surfaces (Augustin-Bauditz et al., 2016; O'Sullivan et al., 2015; Pratt et al., 2009). O'Sullivan et al. (2016) found that ice nucleating proteins from soil can bind onto kaolinite and retain their HIN activity, thus creating an enhanced ice nucleating surface on the dust particle. Despite all this emerging evidence of the existence of a heterogeneous ice nucleating (HIN) bio-dust atmospheric particle mixture, research on quantifying the freezing properties of controlled bio-dust mixtures in the laboratory remains sparse. Recently, Augustin-Bauditz et al. (2016) investigated the mixing state and HIN activity of illite NX mineral dust particles mixed with birch pollen wash water using the Leipzig Aerosol Cloud Interaction Simulator (LACIS). They found that when birch pollen existed on the mineral particle surface, the freezing temperature was determined solely by the biological material. This was concluded from their ability to model the freezing behavior of the mixed experiment using parameters derived from experiments on the individual components. While a seemingly obvious result, it is a worthwhile endeavor to investigate whether a mixture of particle components can produce a new intermediary range of freezing temperatures that isn't observed when each of the INP species is present individually. This helps to determine if the chemical mixing state – the extent to which different chemical components are mixed at the individual particle level – can modify each individual component's distribution of HIN activity, or if the total activity is just a linear addition of that of the individual components. These mixed particle systems also provide a valuable opportunity to evaluate the ability of HIN models such

as our recent $\bar{g}$ framework to predict the freezing properties of mixtures using the properties obtained from the pure components.

1.1 The influence of ice nucleating particle mixing state on droplet freezing temperatures

In Beydoun et al. (2016) the concepts of internal variability and external variability in HIN activity were defined and shown to have a dramatic impact on the temperature range a droplet population freezes in. If the same distribution of HIN activity is contained within each particle in an aerosol population (the internal variability), then the range of temperatures over which these particles cause freezing in the droplets they are contained in would be significantly different than if that same distribution was distributed externally (the external variability). Figure 1a illustrates the concepts of internal versus external variability. In the top right-hand panel of Fig. 1a each droplet contains a particle surface with a color gradient representing the distribution of HIN activity. Note that each particle contains the same distribution of HIN – demonstrating full internal variability – and therefore the range of temperatures over which droplets freeze is relatively narrow, as depicted in the bottom panel. As the surface area of the particle surface in each droplet decreases, the HIN distribution becomes externally variable, meaning that each droplet now contains a different distribution of HIN activity, which is shown with the different colors the particle surfaces are illustrated with in the top left hand panel of Fig. 1a. The reduced surface area per droplet leads to a reduction in the freezing temperatures while the increased external variability leads to a broader temperature range over which droplets freeze relative to the larger surface area case where the variability in HIN activity between each droplet was eliminated.

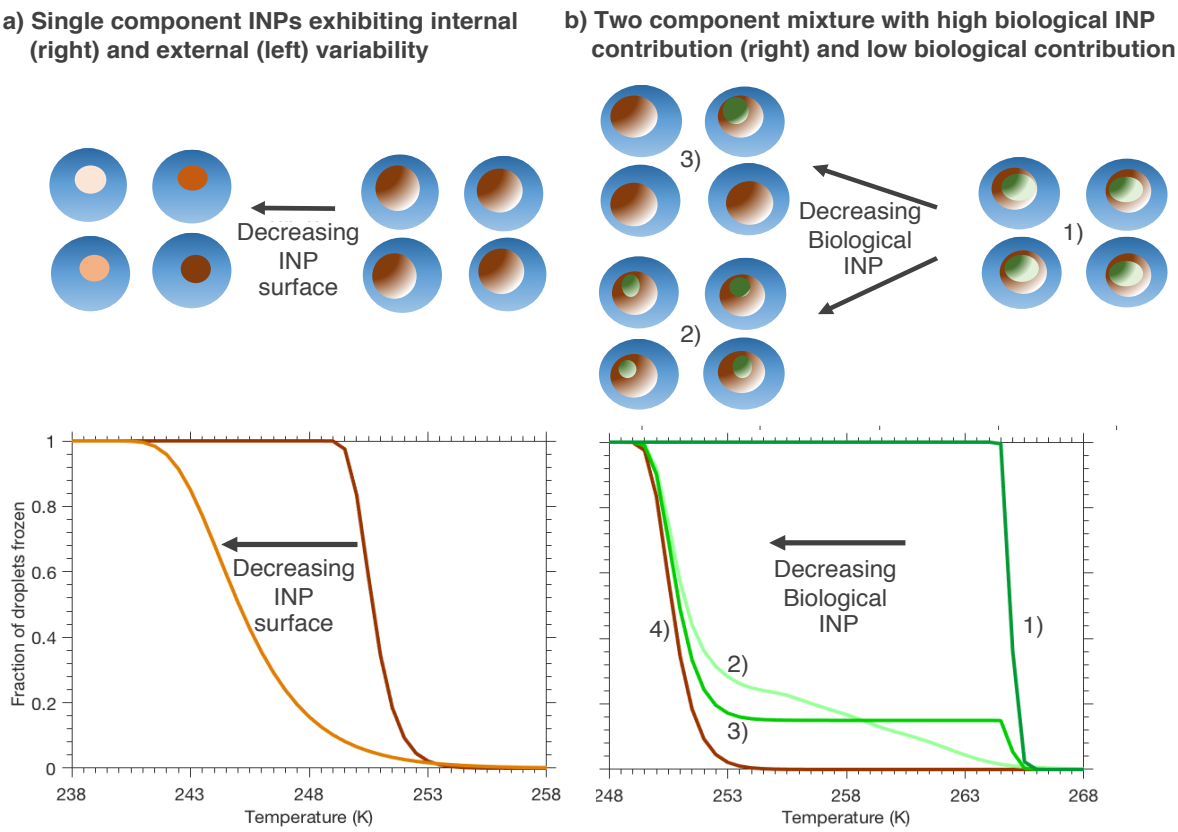

a) Top: Right: Droplets containing particle surfaces larger than the component's critical surface area exhibiting internal variability (color gradient) in HIN activity. Left: Droplets contain particle surfaces smaller than the component's critical surface area and exhibit external variability in HIN depicted by the different colors. **a) Bottom:** Decreasing surface area leads to higher external variability in HIN activity and thus a wider range over which droplets freeze. **b) Top:** Right: Droplets contain a mixture of mineral dust (brown) and biological (green) particle surfaces, both of which are larger than their component's critical surface area. Left: Two hypothetical scenarios of reduced biological particle surface areas are depicted as the concentration of biological INP is reduced. In (2) the biological material distributes itself equally among the droplets and thus remains internally mixed while in (3) the biological material does not further partition itself further and becomes externally mixed. Scenario (4) represents the absence of any biological material (Top right corner of Fig. 1a) and the resultant temperature freezing spectrum is identical to the one for dust lying above its critical surface area shown in the bottom of Fig. 1a. **b) Bottom:** The predicted impact of the INP concentration and mixing state of the dust-bio mixture on the resultant freezing spectrum of droplets containing the particle mixture.

To place the concepts of internal versus external variability in the context of cloud evolution one can consider the example study conducted by Ervens and Feingold (2012) in which different HIN treatments were compared in a cloud air parcel model. A close examination of the impact of variability in HIN activity was performed, whereby different HIN schemes – that inherently make assumptions about whether HIN

activity is externally variable or internally variable – were compared. For example the alpha-PDF scheme (Welti et al., 2012) assumes total external variability, while an internally mixed soccer ball model (Niedermeier et al., 2011) assumes total internal variability. The different schemes resulted in a difference of a factor of 3 in the ice crystal concentration following cloud glaciation. The ice water content distribution with height was also different, whereby the alpha-PDF scheme resulted in higher variability in ice water content versus altitude due to it inducing droplet freezing over a wider temperature and thus altitude range.

While the particle chemical component mixing state and HIN external versus internal variability are not one in the same, the two properties are certainly relatable. If an aerosol particle population is chemically diverse and this diversity is externally distributed, then the freezing capabilities of the entire particle population would need to be defined by many different distributions of HIN activity; each particle would have a different distribution of ice nucleation ability. This becomes more significant with components exhibiting very different HIN properties, such as biological and mineral particles. A completely internally mixed aerosol particle population on the other hand can imply total internal variability in HIN activity; each particle has the same composition and therefore the same ice nucleation ability. In considering illite NX for example, this widely used proxy for atmospheric mineral dust is composed of illite clay along with smaller amounts of kaolinite, quartz, calcite, and feldspars minerals (Hiranuma et al., 2015a). Despite this chemically diverse profile, one distribution of HIN activity $\bar{g}$ was sufficient to accurately describe the freezing behavior of illite NX over many orders of magnitude of particle surface area and consequently a wide freezing temperature range from -20 °C down to -35 °C (Beydoun et al., 2016).

Returning to the bio-dust mixed particles, it is likely that in a totally internally variable mixture the HIN activity is simply determined by the biological particles given their much stronger HIN activity that induces freezing > -10 °C. The top right-hand panel of Fig. 1b illustrates this, whereby each droplet contains both large biological and mineral dust surfaces and the consequent freezing behavior of the droplets is identical to the case of only biological surfaces present. What is less clear is what happens in the limit of very low

biological particle concentrations and relatively high mineral dust particle concentrations. Does the system then behave as an externally mixed system in which the droplets containing biological particles freeze according to the HIN activity of the biological surfaces while the rest of the droplets freeze as dictated by the dust? Or do the low biological particle concentrations generate a new range of freezing temperatures lying between the freezing temperatures of the two individual and separated particle components? These two scenarios are depicted in the left-hand panel of Fig. 1b along with their hypothesized freezing behaviors in the frozen fraction spectrum underneath.

This paper extends the heterogeneous ice nucleation model presented in Beydoun et al. (2016) to droplet systems comprised of different HIN components. In this study, a single component is defined as a particle type which can be treated as having one distribution of HIN activity. The extended treatment is then used to model the freezing behavior of Snomax, a freeze-dried powder manufactured from nonviable *Pseudomonas syringae* bacteria, immersed in droplets and analyzed on a cold plate. Snomax's ice nucleation properties are attributed to large protein aggregates, and it is often used as a proxy for atmospheric biological INP (Pandey et al., 2016; Polen et al., 2016; Wex et al., 2015). It is argued that Snomax is itself a mixture of two components of INP's and necessitates the extended mixing model to properly describe its entire freezing spectrum. The notion that Snomax is a mixture of INPs of different activities is consistent with the hypothesis that the substance is composed of protein aggregates of different sizes and abundances, particularly the Type I and Type III protein aggregates, that exhibit different freezing temperatures (Hartmann et al., 2012; Turner et al., 1990; Yankofsky et al., 1981). The extended model is then applied to a mixture of illite and Snomax at varying concentrations of the latter to examine how well these two different regimes of HIN activity remain indistinguishable when present in the same droplet, and what the consequent atmospheric implications are.

2 Experimental and computational methods

2.1 Experimental ice nucleation measurements

The cold plate assay used to retrieve the freezing spectra for this study is similar to that described by Polen et al. (2016). Some upgrades to the system have taken place, such as the use of a two-stage thermoelectric cooling (TEC) system comprised of an enclosed air-cooled three-stage cascade cold plate (TECA, AHP-1200CAS) mounted below a single-stage TEC module (TETech, VT-127-1.0-1.3-71) and the custom-built cold plate droplet freezing chamber. The cascade cold plate acts as the heat sink while the one-stage TEC modulates the temperature of the cold plate chamber where the droplets reside. An aluminum dish is placed in the chamber inside which a hydrophobic glass coverslip is immersed in squalene oil. An electronic 0.1 μl pipette (Sartorius eLINE) has also been recently introduced to produce droplets of more consistent sizes. This reduces the total particle surface area variability between individual droplets.

A solution of ultapure Milli-Q water and the particle material being investigated was prepared, from which 40-60 0.1 μl droplets were generated (resulting in a 0.02 resolution in the retrieved frozen fraction) using the electronic pipette and placed on the coverslip immersed in the oil. A cooling rate of 1 K/min was used and images of the droplet array were collected at 1 Hz using an optical microscope and CMOS camera. The images were then used to deduce the fraction of droplets frozen at each temperature; frozen droplets appear black. Each freezing experiment was repeated at least twice to confirm that the independently retrieved frozen fractions fall within 1 K (the temperature measurement uncertainty) of each other for each replicate experiment and that the total number of particle/droplet pairings being examined exceeds 100. The samples used in this study were commercial freeze-dried Snomax powder (York International) and illite NX (Arginotec, NX nanopowder) (Hiranuma et al., 2015a). The illite sample is identical to that used in Beydoun et al. (2016) and therefore the HIN properties derived there are reused for the analysis here. The Snomax sample in this study is the same as that analyzed by Polen et al. (2016) whose freezing spectrum was shown to be consistent with the compilation of Snomax cold plate droplet freezing measurements summarized by Wex et al. (2015). Suspensions from which the droplets were generated were prepared by mixing a known mass of the sample (Snomax or illite) with a known volume of ultrapure Milli-Q water to

form a suspension with a specific weight percentage of the sample in water. The droplets containing a mixture of Snomax and illite were generated from a suspension formed by creating a 1:1 mixture from the pure illite and pure Snomax suspensions.

2.2 The critical particle surface area hypothesis, g, and $\bar{g}$

In Beydoun et al. (2016) we started from classical nucleation theory to formulate a framework of heterogeneous ice nucleation which states that any given particle surface can be assigned a distribution of HIN activity, g. g is a continuous normal distribution of contact angles, θ (used as a proxy for the HIN activity at the particle surface-water interface), and determines the probability that a particle induces freezing in a droplet, P_f, at a temperature, T, via:

$$P_f(T) = 1 - \exp\left(-tA\int_0^{\pi} g(\theta)J(\theta,T)d\theta\right) \qquad (1)$$

where t is the time the droplet spent at the temperature T, A is the surface area of the particle, and $J(\theta, T)$ is the heterogeneous ice nucleation rate per unit surface area per unit time as defined in Zobrist et al. (2007). The freezing probability can also be written for a droplet undergoing a constant cooling rate $\dot{T}$ as:

$$P_f = 1 - \exp\left(-\frac{A}{\dot{T}}\int_{T_i}^{T_f}\int_0^{\pi} g(\theta)J(\theta,T)d\theta dT\right) \qquad (2)$$

For a large ensemble of droplets containing identical particle surfaces, the freezing probability is equal to the fraction of droplets frozen, F.

We hypothesized that an individual particle type possesses a critical surface area, above which one normal distribution of HIN activity $\bar{g}$ can accurately describe the freezing probability of a droplet containing any particle of that type. Therefore, the freezing probability of a droplet containing a particle with a surface area larger than this critical area can be evaluated using Eqns. (1) or (2) with $\bar{g}$ in place of g, and the fraction of

droplets frozen, F, of a large ensemble of these droplets N is equal to the freezing probability of each droplet, P_f. On the other hand, when a particle possesses a surface area below that type's critical surface area, a random sampling of contact angles to generate a discrete distribution of HIN activity g^* is required for each particle surface in the particle population. In this case the frozen fraction of a large ensemble of droplets, F, is the arithmetic mean of the individual droplet freezing probabilities and can be evaluated using:

$$F = \frac{1}{N}\sum_{i=1}^{N} P_{f,i}\left(g^*{}_i(n_{draws})\right) \qquad (3)$$

where $P_{f,i}$ is the freezing probability of droplet i and can be evaluated using Eqns. (1) and (2) with g^* used in place of g and n_{draws} is the number of contact angle draws made from $\bar{g}$. The effect of decreasing an INP's total surface area below its critical surface area threshold on the distribution of HIN activity contained in each droplet is illustrated in Fig. 1 by the extensive broadening of the droplet freezing temperature curve when below the critical area. Above the critical area the diversity of HIN activity is essentially eliminated across the particle population; the large available surface area guarantees that the full distribution of HIN activity is contained in each droplet and described by $\bar{g}$. The creation of the g^* distribution by taking n_{draws} from $\bar{g}$ accounts for this increased diversity in HIN activity when below the critical area threshold.

2.3 Mixing model

The mixing model extends the HIN framework reviewed above to account for multiple distributions of ice nucleation activity presented by multiple INP types inside a single droplet, as well as the contribution from homogenous ice nucleation. It is assumed that every freezing probability is independent of the other, an approach similar to that taken by Augustin-Bauditz et al. (2016) and Broadley et al. (2012) for a mixture of birch wash water pollen and illite NX, and a mixture of illite NX and kaolinite, respectively. The freezing probability of an individual droplet containing some mixture of components $n_c + n_{sc}$, where n_c is the number

of components with surface areas greater than their corresponding critical surface areas and n_{sc} is the number of components with surface areas lower than their corresponding critical surface areas, is:

$$P_f = 1 - P_{uf,hom} \prod_{k=1}^{n_c} P_{uf,c,k}(\bar{g}_k, A_k) \prod_{j=1}^{n_{sc}} P_{uf,sc,j}(g^*{}_j, A_j) \qquad (4)$$

where $P_{uf,hom}$ is the probability freezing does not occur due to homogenous nucleation, $P_{uf,c,k}$ is the probability freezing does not occur due to component k possessing a surface area A_k lying above this component's critical area and thus can be evaluated with $\bar{g}_k$. $P_{uf,sc,j}$ is the probability freezing does not occur due to component j possessing a surface area A_j lying below this component's critical surface area and thus requires random sampling from $\bar{g}_j$ to generate g_j^* for evaluation.

For a large ensemble of N droplets, the frozen fraction F is the mean of the individual droplet freezing probabilities. This yields the following expression for the frozen fraction of droplets:

$$F = 1 - \frac{1}{N} \sum_{i=1}^{N} \left| \exp\left(-\frac{1}{\dot{T}} \int_{T_i}^{T_f} \left(J_{hom} V + \sum_{k=1}^{n_c} A_k \int_0^{\pi} \bar{g}_k(\theta) J(\theta, T)\, d\theta \right.\right.\right.$$
$$\left.\left.\left. + \sum_{j=1}^{n_{sc}} A_j \int_0^{\pi} g^*{}_{i,j}\left(\bar{g}_j, n_{draws,j}\right) J(\theta, T) d\theta \right) dT \right) \right| \qquad (5)$$

where $\dot{T}$ is the cooling rate, T_i and T_f are the initial and final temperatures in a cooling experiment, J_{hom} is the homogenous nucleation rate, V is the droplet volume, and $n_{draws,j}$ is the number of times random sampling takes place from $\bar{g}_j$. An additional subscript i is added to g^* to indicate that the sub-critical area distribution of contact angles (θ) for a component k will vary between droplets. It should be mentioned that derivations of and expressions similar to Eq. (5) can be carried out for any of other existing HIN frameworks starting from the assumption of independent freezing probabilities induced by each component.

For the purposes of the analysis of the experiments presented in this paper, Eqn. (5) can be reduced to describe one component exhibiting behavior above its critical area, one component exhibiting behavior below its critical area, and the background HIN distribution of impurities in the species being examined or the milli-Q water itself. The latter process does not strictly proceed through homogenous ice nucleation and causes freezing to happen at a much higher temperature than the expected homogeneous freezing temperature range of the 400-600 μm droplets used in this study. Eqn. (5) is thus reduced to:

$$F = 1 - \frac{1}{N}\sum_{i=1}^{N}\left[\exp\left(-\frac{1}{\dot{T}}\int_{T_i}^{T_f}\left(A_1\int_0^{\pi} g^*_{i,1}(\bar{g}_j, n_{draws,j})J(\theta,T)d\theta + A_2\int_0^{\pi}\bar{g}_2(\theta)J(\theta,T)\,d\theta + \int_0^{\pi}G_{bg}(\theta)J(\theta,T)d\theta\right)dT\right)\right] \quad (6)$$

It should be noted that the distribution of ice nucleating activity of the background impurities has been lumped with its implied particle surface area into one term $G_{bg.}$ This simplification serves the same purpose of simply accounting for droplet freezing that could be occurring due to background impurities. The contribution from this term becomes particularly important at low particle concentrations. G_{bg} is thus a normal distribution multiplied by a pre-factor making it a function of three independent parameters: the pre-factor (C), the mode (μ), and the standard deviation (σ).

3 Results and discussion

3.1 Snomax: Two distributions of heterogeneous ice nucleating activity

The HIN behavior of Snomax was investigated by varying the concentration of the prepared particle suspension to retrieve the full freezing temperature spectrum of the system. Similar droplet freezing measurements of Snomax have been conducted and analyzed before as summarized in Wex et al. (2015). However, the analysis presented here is unique due to the application of the newly developed critical area method we presented in Beydoun et al. (2016) and summarized above. Freezing spectra for Snomax mass concentrations of $1x10^{-1}$, $5x10^{-2}$, $3x10^{-2}$, $1x10^{-2}$, $5x10^{-3}$, $1x10^{-3}$, $5x10^{-4}$, $1x10^{-4}$, $5x10^{-5}$, $1x10^{-5}$, and $1x10^{-6}$ wt%

were obtained and are plotted in Fig. 2a. Figure 2b extends Fig. 2a to show the freezing spectra corresponding to Snomax mass concentrations of $5x10^{-7}$ and $1x10^{-7}$ wt%.

For Snomax concentrations of $1x10^{-1}$wt% through $5x10^{-4}$ wt% the temperatures over which droplets freeze gradually broadens and decreases as the concentration is decreased. This is consistent with the trend observed with the systems analyzed in Beydoun et al. (2016) in which the broadening is interpreted as particle surface areas becoming smaller than the species' critical area, which creates external variability in the HIN activity of the particle surface available in each droplet. The highest two concentrations ($1x10^{-1}$and $5x10^{-2}$ wt%) can be fit with the same g distribution. The solid lines in Fig. 2a indicate a single g fit. A least squares error approach is used to find the g distribution of θ (μ, σ) that best models the highest concentration freezing curve and this g is then reused to predict the second highest concentration freezing curve, following the procedure outlined in Beydoun et al. (2016). At concentrations lower than $5x10^{-2}$ wt% a single g fit fails at predicting the behavior of the freezing curves. The behavior is defined by the median freezing temperature at which 50% of the droplets freeze and the range of temperatures over which droplets freeze. A failed fit produces a freezing curve that is not within the 1 °C experimental temperature uncertainty of each experimental frozen fraction data point. The successful fitting of the frozen fraction curves at the two highest Snomax concentrations ($1x10^{-1}$and $5x10^{-2}$ wt%) using one g distribution suggests that the particle surface areas inside the droplets fall above the critical surface area threshold. Therefore, the g retrieved is $\bar{g}$. Conversely the emergence of the broadening trend in freezing temperatures with decreasing Snomax concentration starting with the $3x10^{-2}$ wt% frozen fraction curve suggests that particle surface areas inside each droplet lie below the critical area threshold and consequently exhibit external variability in their HIN

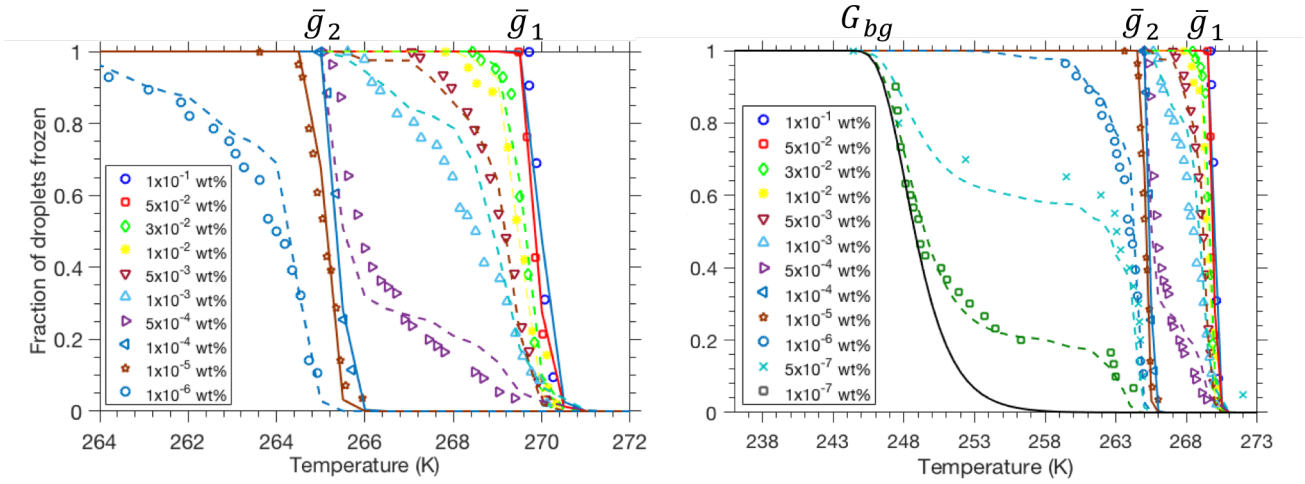

Figure 2. a) Frozen fraction temperature spectra for Snomax mass concentrations of 1x10^{-1}, 5x10^{-2}, 3x10^{-2}, 1x10^{-2}, 5x10^{-3}, 1x10^{-3}, 5x10^{-4}, 1x10^{-4}, 1x10^{-5}, and 1x10^{-6} wt% (symbols). Critical area fits using two distinct Snomax distributions of HIN activity (solid lines) are shown for some droplet freezing curves, while the rest of the freezing curves are modelled with the mixing model (dashed lines). **b)** All frozen fraction curves shown in a) in addition to the lowest Snomax concentration frozen fraction curves of 5x10^{-7} and 1x10^{-7} wt%. The lowest concentration freezing curves are modelled using random sampling by n_{draws} of the $\bar{g}_2$ distribution of HIN activity. The solid black line is the assumed frozen fraction curve induced by the background impurities in the droplets.

activity. The broadening trend continues with decreasing particle concentration until the 1x10^{-4} wt% Snomax concentration, whereby a steep freezing curve with a narrow range of freezing temperatures re-emerges. The g_2 distribution that fits this low concentration freezing curve is a different Gaussian function than the g_1 distribution that fits the first two high concentration freezing curves (after accounting for the change in particle surface area). Furthermore, the g_2 distribution obtained from the 1x10^{-4} wt% freezing curve also fits the 1x10^{-5} wt% freezing curve before a new trend of frozen fraction curve broadening emerges starting with the 1x10^{-6} wt% concentration. Figure 1b expands the temperature range of the frozen fraction curves to show the unique trend of the very low concentration freezing curves (5x10^{-7} and 1x10^{-7} wt%). Only the initial part of these frozen fraction curves exhibits broadening and freezing at high temperatures beyond which there is an approximate plateau without further droplet freezing between 263 and 253 K. The plateau ends around a similar temperature range between 253 K and 248 K for both low particle concentrations and they converge around what is probably freezing due to background impurities in the water, the sample, or the hydrophobic coverslip. These background impurities will be discussed in more detail later in this section.

Based on these observations, it is hypothesized that Snomax can be modelled as having two distinct distributions of HIN activity, each possessing its own critical surface area threshold. Using the fits to the frozen fraction curves of the $1x10^{-1}$ and $5x10^{-2}$ wt% Snomax concentrations, the first distribution denoted $\bar{g}_1$ is a normal distribution with parameters $\mu_1 = 0.60$ and $\sigma_1 = 0.050$ (Eqn. (2)). Similarly, the fits to the frozen fraction curves of the $1x10^{-4}$ and $1x10^{-5}$ wt% Snomax concentrations give the second distribution of HIN activity denoted $\bar{g}_2$ with parameters $\mu_2 = 0.52$ and $\sigma_2 = 0.0001$. This can be viewed as a mathematical interpretation of Snomax's hypothesized Type I and Type III proteins, which are said to cause freezing at similar temperature regimes to where the first and second critical areas have been identified from the freezing spectra in Fig. 2 (Turner et al., 1990; Yankofsky et al., 1981). For this analysis it is assumed that all HIN components of Snomax have surface area densities of 1 m^2/g. While not based on an empirical value, the surface area density assumption is merely invoked since the model is set up such that freezing probabilities are evaluated as a function of surface area and not mass. The assumption does not affect the insight gained from the analysis. This results in $1x10^{-5}$ cm^2 and $1x10^{-8}$ cm^2 for the first and second critical surface areas thresholds, respectively, of the $\bar{g}_1$ and $\bar{g}_2$ distributions of HIN activity. Note that the $\bar{g}_1$ is responsible for the freezing observed at higher temperatures when higher Snomax concentrations are used.

The Snomax particle concentrations of $3x10^{-2}$ through $5x10^{-4}$ wt% that correspond to the frozen fraction curves between the two steep sets of frozen fraction curves are thus considered to possess surface areas between the critical area thresholds of the first and second distribution of Snomax INP's, whose HIN activity are described by $\bar{g}_1$ and $\bar{g}_2$. Modelling these freezing curves is thus the first application of the extended mixing model summarized in Eqn. (6) as there are two distinct and distinguishable types of INPs present in droplets containing Snomax particles. The g^* distributions describe the more-active $\bar{g}_1$ HIN type for which the Snomax concentrations are below its critical area threshold. The g^* distributions used in the first term inside the exponential in Eqn. (6) are retrieved by taking a number of random θ values, n_{draws}, from $\bar{g}_1$, whereby each frozen fraction curve will have a unique n_{draws} that produces a modelled frozen fraction curve

closest to the measured curve. The random sampling process is repeated up to three times to ensure repeatability of the modelled frozen fraction curve. The optimization of n_{draws} is carried out manually as the range of n_{draws} which results in changes to the modelled frozen fraction curves is small enough such that a more comprehensive numerical optimization (e.g. a Monte Carlo simulation) was not found to be necessary. In the case of the mixture of two distributions of HIN activity in Snomax, A_1 is assumed equal to A_2 and is calculated from the Snomax concentration and the assumed surface area density. The last term corresponding to the HIN activity of background impurities can be safely neglected here as the freezing temperatures are much higher than temperatures at which background impurities typically cause freezing in this system (< 248 K). The consequent n_{draws} for each frozen fraction curve between the two Snomax critical areas are: 80 for the $3x10^{-2}$ wt%, 65 for $1x10^{-2}$ wt%, 40 for $5x10^{-3}$ wt%, 25 for $1x10^{-3}$ wt%, and 6 for $5x10^{-4}$ wt%. The modelled frozen fraction curves are plotted as dotted lines in Figs. 2a and 2b.

Modelling the frozen fraction curve for the lowest concentration frozen fraction curve lying between the two critical surface areas ($5x10^{-4}$ wt% Snomax concentration) necessitated placing a lower contact angle limit when conducting random sampling. At a low number of n_{draws} it becomes likely that some g^* distributions become unrealistically active due to over sampling of lower contact angles and consequent normalization of the distribution as outlined in Beydoun et al. (2016). Therefore, a lower contact angle limit of $\theta = 0.220$ radians was invoked for modelling this frozen fraction curve. It should also be mentioned that the choice of this lower contact angle limit is not arbitrary as it is based on a nucleating surface area analysis introduced in Beydoun et al. (2016) of the highest concentration frozen fraction curve (0.1 wt% Snomax) in which it was found that 0.220 radians approximated a critical contact angle below which contact angles do not comprise an appreciable surface area to contribute to nucleation. Therefore, if any θ smaller than 0.220 does not contribute to freezing at particle surface areas above the critical surface area threshold then it should not contribute to freezing for surface areas below it. It should be emphasized that this special invocation was only done for modelling one of the frozen fraction curves in the entire study. This last point is a recognized

caveat of the model and improvements to the numerical technique to be more consistent across the entire range of n_{draws} is a subject of ongoing research.

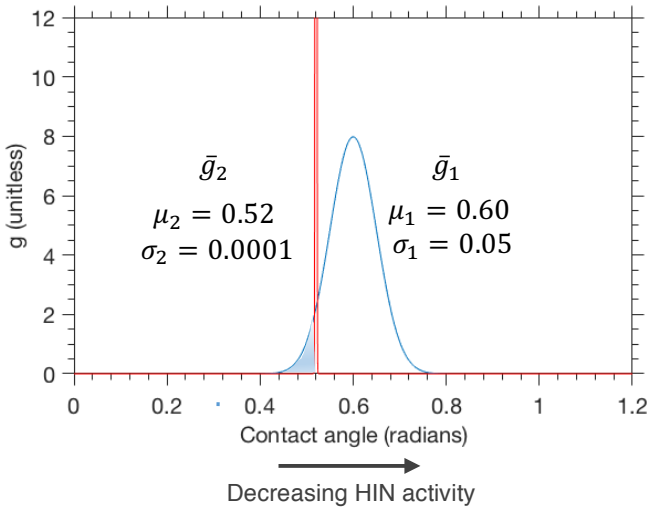

Figure 3. The two distributions of HIN activity, $\bar{g}_1$ (right, broad, in blue) and $\bar{g}_2$ (left, narrow, in red), retrieved from the Snomax droplet freezing spectra (Fig. 2).

A similar analysis was performed to model the frozen fraction curves with surface areas below the second critical area threshold, which correspond to Snomax concentrations of $1x10^{-6}$, $5x10^{-7}$, and $1x10^{-7}$ wt%. In this case Eqn. (6) is used without the contribution from a component with a surface area larger than its own critical area threshold (the second term inside the exponential). Random sampling to produce the g^* distributions is done from $\bar{g}_2$, which was determined using the $1x10^{-4}$ and $1x10^{-5}$ wt% Snomax curves as described above. The HIN activity of background impurities has an important contribution for these low concentrations as can be seen in Fig. 2b by the fact that all three of these frozen fraction curves with surface areas below the second critical surface area threshold finish freezing along the same low temperature freezing line. This freezing line is assumed to be due to the HIN activity of the background impurities. It should be noted however that this freezing line is not reproducible when retrieving the frozen fraction curve of droplets made up only of Milli-Q water, which freeze 5 K colder than this line. It was also not possible to reproduce this background freezing spectrum with a newly acquired batch of Snomax, whereby droplets containing particle material from the new batch froze at a lower temperature than the droplets containing particle material from the old batch. Therefore, it is likely that these impurities are associated with this particular

Snomax sample, so their resultant frozen fraction curve will simply be added to the mixing model in the form of G_{bg}. G_{bg} is derived by extrapolating the low temperature part of the frozen fraction curve of the lowest Snomax concentration (solid blue line in Fig. 1b). The resultant parameters are $\mu_{bg} = 2.8$ and $\sigma_{bg} = 0.25$ and a pre-factor $C = 2.5\text{x}10^{-6}$. The consequent n_{draws} for each frozen fraction curve below the second Snomax critical area threshold are: 8000 for $1\text{x}10^{-6}$ wt%, 2800 for $5\text{x}10^{-7}$ wt%, and 750 for $1\text{x}10^{-7}$ wt%. The much higher n_{draws} values for this range of concentrations are due to the much narrower range of HIN activity that distribution $\bar{g}_2$ covers compared to distribution $\bar{g}_1$ (σ_2 is much smaller than σ_1, 0.0001 versus 0.05). A larger number of draws from $\bar{g}_2$ is therefore required to capture its HIN activity.

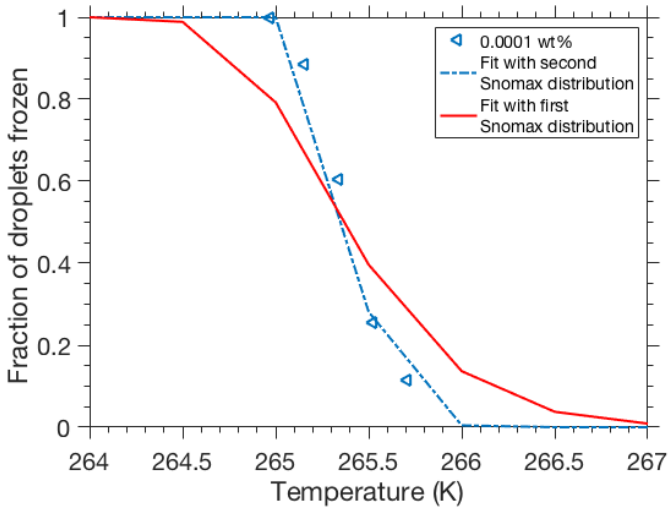

Figure 4. The $1\text{x}10^{-4}$ wt% Snomax frozen fraction curve (symbols), corresponding to the highest concentration freezing spectrum where freezing was exclusively determined by the $\bar{g}_2$ distribution of HIN activity. Freezing spectra fits are also included, one derived using the $\bar{g}_2$ distribution of HIN activity (dashed line), while the other is a hypothetical fit corresponding to the activity of the $\bar{g}_1$ distribution (solid line).

Figure 3 shows the two Snomax $\bar{g}$ distributions plotted alongside each other for comparison. The first striking contrast lies in the σ value for each distribution ($\sigma_1 = 0.05$ vs. $\sigma_2 = 0.0001$), which defines the range of contact angles a g distribution covers. Typically, a larger σ does lead to a broader range of freezing temperatures when the surface area is larger than its critical area. However, for the same σ, frozen fraction curves at higher temperatures are steeper (exhibit freezing over a narrower temperature range) than at lower temperatures, due to the strength of the range of HIN activity causing higher temperature freezing. The

temperature range where freezing ensues is determined by the distribution of contact angles, which is governed by both μ and σ. While merely looking at the frozen fraction curves dictated exclusively by either $\bar{g}_1$ or $\bar{g}_2$ in Fig. 2 would hint at similar HIN activity contact angle breadth, it should be emphasized that the contact angle range for $\bar{g}_2$ must be narrower (smaller σ) and/or have a larger mode value, μ, due to it causing freezing at lower temperatures. In other words, if $\bar{g}_1$ was used to try and fit the frozen fraction curves associated with $\bar{g}_2$, the consequent fit would not only overpredict the freezing temperature but also the range of temperatures over which freezing would occur. Figure 4 shows a fit for the $1x10^{-4}$ wt% frozen fraction curve that uses $\bar{g}_1$ instead of $\bar{g}_2$. The required surface area input for this alternative fit of the $1x10^{-4}$ wt% frozen fraction curve is smaller by a factor of 10^{-8} than the surface area used for the $1x10^{-1}$ wt% frozen fraction curve, when it should only be smaller by a factor of 10^{-3} based on the differences in Snomax mass concentration of each curve. Furthermore, the range of temperatures over which freezing occurs using $\bar{g}_2$ is noticeably broader for the fit using $\bar{g}_1$, which supports the point made above.

A narrower σ for the $\bar{g}_2$ distribution is also reflected in the very abrupt transition in freezing behavior that droplets containing low Snomax concentrations undergo with decreasing concentration. As depicted in Fig. 2b, after a second Snomax critical area regime determined exclusively by $\bar{g}_2$ that covers 2 orders of magnitude in concentration ($1x10^{-4}$ and $1x10^{-5}$ wt%) a sub-critical area regime begins (the broader $1x10^{-6}$ wt% frozen fraction curve) followed by a very quick transition (after only a factor of 5 concentration decrease) to a loss of Snomax HIN activity in at least 60% of the droplets ($5x10^{-7}$ wt% frozen fraction curve). While frozen fraction curves lying between critical area 1 and critical area 2 covered two orders of magnitude in concentration before partial loss of HIN activity represented by $\bar{g}_1$, frozen fraction curves lying below critical area 2 covered only one order of magnitude. Furthermore, the continually dominant contribution from the contact angle range causing freezing at a high temperature of about 265 K to 263 K also points to a narrow second distribution of HIN activity. This can be seen in the transition between Snomax concentrations of $1x10^{-6}$ wt% to $5x10^{-7}$ wt% and $1x10^{-7}$ wt% whereby the two lowest concentration freezing curves exhibit

most of their freezing at the higher temperatures (265 K-263 K) of the temperature range the second distribution of HIN contributes to (Fig. 2b). However, it should be noted that the existence of some broadness in the temperature over which droplets freeze throughout the regime falling below the second critical area does necessitate that $\bar{g}_2$ still has a finite σ, albeit a small one.

The second notable feature in the contrast between the two Snomax distributions of HIN activity shown in Fig. 3 is that the mode of the less active $\bar{g}_2$ distribution ($\mu_2 = 0.52$) is actually at a smaller contact angle (i.e. more ice active) than that of the $\bar{g}_1$ distribution ($\mu_1 = 0.60$). This is not contradictory to the resultant freezing curves where the INP's represented by $\bar{g}_1$ cause freezing at several degrees warmer than those of $\bar{g}_2$. The freezing temperatures are actually determined by the ascending tail of the first distribution for the droplets containing high Snomax concentrations (dashed portion of the $\bar{g}_1$ curve shown in Fig. 3). The tail of the broader $\bar{g}_1$ distribution spreads into a lower (more active) contact angle range than the much narrower $\bar{g}_2$ distribution does. Furthermore, the broader $\bar{g}_1$ distribution of HIN activity can be interpreted as being consistent with the finding by Polen et al. (2016) that the more active Type I protein aggregates (which are described by the first distribution, $\bar{g}_1$) are less stable over storage time and refreezes than the Type III protein aggregates (which are described by the second distribution, $\bar{g}_2$). A broader distribution implies that freezing is determined by a wider (more variable) range of HIN activity and thus a wider diversity of the INP's properties. The freezing induced by the more active $\bar{g}_1$ distribution is understood to be caused by rare and very active large proteins aggregates that would arguably be more susceptible to deterioration, weakening, and decay over time. This would produce a wider diversity in HIN activity, which would result in the broader $\bar{g}_1$ normal distribution of contact angles (Fig. 3) that we derived from analysis of the droplet freezing spectra in Fig. 2.

3.2 Mixtures of Snomax and Illite particles

The second part of this study investigates the applicability of the mixing model to a mixture of Snomax bacterial and illite mineral particles, recalling that Snomax is itself a mixture of at least two distinct types of INPs. Figure 5 shows two droplet freezing spectra retrieved from droplets generated from a mixture of Snomax and illite: a 1:1 mixture of $5x10^{-7}$ wt% Snomax and 0.1 wt% illite, and a 1:1 mixture of $1x10^{-7}$ wt% Snomax and 0.1 wt% illite. The two frozen fraction curves are plotted along with the other Snomax frozen fraction curves and another spectrum retrieved from a 0.05 wt% illite suspension. As the Snomax-illite mixtures were prepared by mixing equal amounts of each component, the effective concentration of each is half its original concentration. That is why a 0.05 wt% illite frozen fraction curve is included in Fig. 4 as it should better resemble the illite concentration in the mixture. It was shown in Beydoun et al. (2016) that for

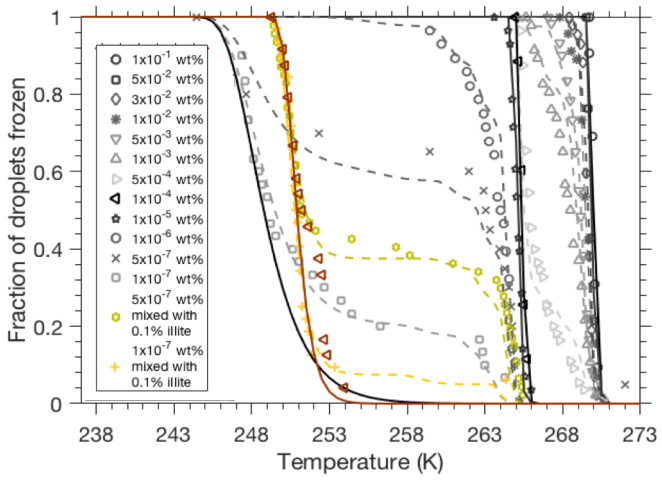

Figure 5. All droplet freezing spectra for Snomax-containing droplets from Fig. 1 shown in grey, along with the frozen fraction curves corresponding to 0.05 wt% illite (dark red), a 1:1 mixture of $5x10^{-7}$ wt% Snomax and 0.1 wt% illite (yellow), and a 1:1 mixture of $1x10^{-7}$ wt% Snomax and 0.1 wt% illite (orange). The modelled frozen fraction curve for the 0.05 wt% illite frozen fraction curve is also plotted (solid dark-red line) along with the fits for the frozen fraction curves corresponding to the illite-Snomax mixtures (yellow and orange dashed lines). Solid black lines on the right are frozen fraction curves that can be described by a $\bar{g}$ distribution ($\bar{g}_1$and $\bar{g}_2$). The solid black line on the left is the modelled frozen fraction curve of the background impurities.

this method and a 0.03 wt% illite concentration, the resultant freezing curve can be modeled using illite's previously retrieved $\bar{g}$ ($\mu_{illite} = 1.72, \sigma_{illite} = 0.122$) and surface area of $A_{\text{illite}} = 2.0 \times 10^{-2}$ cm^2. Illite is above its critical area threshold at this concentration. This predicted curve using illite's $\bar{g}$ distribution is also shown

in Fig. 5. At this concentration, illite does not induce freezing until < 254 K, well below the critical temperature range of Snomax's weaker $\bar{g}_2$ distribution that is observed > 260 K.

The mixing model expressed by Eqn. (6) is applied to the droplet frozen fraction curves corresponding to the mixtures of Snomax and illite. In this case the contribution from the background impurities is ignored, which is thought to be a good assumption as the tail of the frozen fraction curves aligns quite well with the frozen fraction curve for droplets containing only 0.05 wt% illite. Random sampling takes place from $\bar{g}_2$ for Snomax to produce the g^* distributions needed for the first term inside the exponential in Eqn. (6) since these Snomax concentrations are below the $\bar{g}_2$ distribution's critical area threshold, while the second term uses $\bar{g}_{illite}$ and A_{illite} that were previously determined as discussed above for illite above its critical area. The consequent n_{draws} values that result in the closest modelled frozen fraction curves for each of the experimental frozen fraction curves produced from a Snomax-illite mixture are: 1190 for $5\text{x}10^{-7}$ wt% Snomax mixed with 0.1 wt% illite, and 500 for $1\text{x}10^{-7}$ wt% Snomax mixed with 0.1 wt% illite. The model produces frozen fraction curves that encompass the freezing behavior observed for the Snomax-illite mixtures quite well, with an initial increase in the fraction of droplets frozen due to the contribution from the HIN activity of Snomax in the same way the frozen fraction of droplets containing only Snomax behaved. This is followed by an approximate plateau in the frozen fraction curve indicating the absence of any Snomax INPs. It should be noted that the reduction in the intermediary plateau of the fraction of droplets frozen containing the Snomax-lllte mixture compared to the droplets containing only Snomax can be explained by the reduction of effective Snomax concentration in the mixture due to diluting the concentrations of the 0.1 wt% illite and the $5\text{x}10^{-7}$ wt% Snomax as well as the $1\text{x}10^{-7}$ wt% Snomax by half upon making 1:1 solutions of each. While Augustin et al. (2016) speculated that the reduction in freezing temperatures upon mixing birch pollen wash water with an illite solution may have had to do with the resultant mixing state of the generated particles, no evidence of this is found in our measurements. The mixing model presented here is therefore only the second HIN model that accounts for multiple independent distributions of HIN, and the first to do so for a system comprised of four distinct distributions of HIN activity (the two distributions of HIN activity of Snomax, that

of illite, and that of the background impurities) spanning seven orders of magnitude of particle material concentration and a temperature range of 271 K down to 248 K.

Due to Snomax's well-defined cutoff in HIN activity at low concentrations where no freezing is induced below 258 K, there is really no temperature regime in which the INP's contained in illite and Snomax compete. In other words, it is not possible to dilute Snomax to a point where its HIN activity is expressed in the temperature range where illite's HIN activity becomes significant. The measurements do clearly indicate that there is a high temperature cutoff for Snomax's contribution to freezing and the mixing model does a good job of producing this behavior.

A droplet-particle system examined here that deserves greater attention is the 1:1 mixture of $1x10^{-7}$ wt% Snomax and 0.1 wt% illite. At this effective Snomax concentration of $5x10^{-8}$ wt%, the volume equivalent diameter of total surface area of Snomax particles present is around 550 nm (for an assumed 1 g/cm^3 density). Hartmann et al. (2013) investigated the HIN activity of size selected Snomax particles using the LACIS cloud simulator (Stratmann et al., 2004). Their results were somewhat consistent with what was found here as their 650 nm and 800 nm size-selected particles produced a frozen fraction curve that plateaued at 10% of droplets frozen below 263 K. Smaller Snomax particle sizes they investigated (100 nm, 300 nm, 400 nm) caused freezing at lower temperatures between 263 K and 258 K and were generally found to be rarer than the larger particles in the polydisperse aerosol size distribution. This may explain why upon decreasing the Snomax concentration in the experiments presented here, the droplets retained freezing at the higher temperatures of 265 K to 263 K and not the lower temperatures of 263 K to 258 K as shown in frozen fraction curves corresponding to droplets containing $1x10^{-7}$ wt% Snomax, and $1x10^{-7}$ wt% Snomax mixed with 0.1 wt% illite. Therefore, in the context of atmospheric aerosol, at the limit of a very low probability of finding a biological particle, the INP's represented by the less active but more abundant Snomax $\bar{g}_2$ distribution and their colder critical temperatures are the most likely to be found (in the limiting assumption of Snomax being a reasonable proxy of biological INPs). This is what the lower Snomax concentration frozen fraction curve

associated with the Snomax-illite mixture resembles; even when Snomax particles become scarce they still induce a high freezing temperature in the small fraction of droplets that still contain them (around 5% in the frozen fraction curve being examined).

The question then of what ratios of Snomax and illite are needed for one to control the HIN activity over the other becomes irrelevant. The existence of any Snomax particles in a droplet will shift the resultant freezing to a much higher temperature regime and no amount of mineral dust can practically compete with that. This understanding provides more quantitative validation of the conventional wisdom that a relatively rare biological particle exhibits exceptional freezing behavior, overwhelming other non-biological components. Augustin et al. (2016) provided evidence of this but it remained unclear whether the illite in the illite/birch pollen wash water mixture investigated was contributing to freezing at all, as the resultant frozen fraction curve of the mixture merely looked like a weaker version of the frozen fraction curve retrieved from the droplets comprised purely of birch pollen wash water (identical shape but with a lower freezing temperatures). This arguably limits the ability to validate a mixing model to a system comprised of a mixture of INPs. It could also be argued that probing only one size and thus surface area of INPs in their study is another limitation and varying these parameters could have helped discern whether differences in the resultant frozen fraction curves between the mixtures and the pure components were due to differences in the amount of INP material present or due to potential mixing state alteration.

From the perspective of modelling multi-component heterogeneous ice nucleating particles, it remains a subject of further research to determine how many $\bar{g}$ distributions are necessary to encompass the freezing behavior of mixed particle systems at low temperatures where dust is known to be quite ice active. However, the work presented here supports the notion that two distributions of HIN activity are necessary to distinguish between the dust and biological regimes when illite and Snomax are used as proxies for these two types of INP. Regarding the motivating hypothesis that small biological particles can enhance the freezing capabilities of mineral dust surfaces, it can be concluded that the effectiveness of Snomax enhancing illite or any mineral

dust surface is limited by its ability to partition itself and thus allow its HIN activity to be manifested externally. Hypothetical scenario 3, that was introduced in Section 1.2 and depicted in Fig. 1b, in which the limited amount of biological material does not distribute itself among all droplets, therefore closely resembles the bio-dust mixture proxy examined here. This is in contrast to the more effective behavior of soil borne fungus investigated in O'Sullivan et al. (2016). The biological macromolecules in that study were shown to bind onto clay and thus partition themselves among the dust surfaces, thereby distributing their HIN activity externally. This difference between Snomax and soil borne fungus should be kept in mind when considering the relevance of dust-bio mixtures in the atmosphere, and future work can attempt to quantify whether the ability of soil born fungus to adsorb unto clay surfaces can render it a stronger INP than Snomax despite its weaker HIN activity.

4. Conclusions

A new heterogeneous ice nucleation (HIN) mixing model was formulated to better understand and predict how cloud droplet systems containing more than one component or type of INPs behave. The new model successfully predicted the freezing spectra of droplets containing Snomax bacterial particles as well as a mixture of Snomax and illite NX mineral particles, a proxy for bio-dust particle mixtures in the atmosphere. Snomax was characterized by two distributions of HIN activity, a model consistent with Snomax's proposed ice nucleating Type I and Type III protein aggregates. The first distribution exhibited a broader contact angle range and therefore had a more gradual decay in its contribution to droplet freezing with decreasing concentration compared to the second distribution that exhibited a very narrow range of contact angles. The broadness of the first distribution is likely related to the INPs' instability as the very rare and most active Snomax INPs can noticeably deteriorate over time as recently reported by Polen et al. (2016).

Upon examining droplets containing a mixture of illite mineral particles and a low concentration of Snomax, the resultant frozen fractions merely followed freezing as dictated by the HIN activity of each individual component; there was no evidence of an intermediary freezing temperature range produced by

mixing the two types of INPs. This result is similar to the one reported in Augustin-Bauditz et al. (2016) using a mixture of birch pollen wash water and illite. The absence of a broad range of nucleating temperatures connecting the two HIN regimes is partly due to the sharpness of the second Snomax distribution of HIN activity. The inability of Snomax bacterial particles to further distribute themselves externally among all droplets is what led the mixture to exhibit the two distinct regimes of freezing due to Snomax and illite, respectively. Therefore, in the limiting assumption that the system examined here is a close proxy to real atmospheric bio-dust mixtures, it would be safe to assume that the limiter to high temperature heterogeneous freezing in the atmosphere is merely the existence of biological material in the droplet. More likely than not no compromise would be made in the quality of biological material's HIN activity when freezing is induced due to the presence of other particle components, such as the illite minerals studied here.

Acknowledgements. This research was supported by the National Science Foundation (CHE-1554941). Hassan Beydoun was partially supported by the Bertucci Fellowship from the College of Engineering at Carnegie Mellon University. Michael Polen was supported by a Graduate Research Fellowship from the National Science Foundation.

References

Ariya, P. A., Sun, J., Eltouny, N. a., Hudson, E. D., Hayes, C. T. and Kos, G.: Physical and chemical characterization of bioaerosols – Implications for nucleation processes, Int. Rev. Phys. Chem., 28(1), 1–32, doi:10.1080/01442350802597438, 2009.

Atkinson, J. D., Murray, B. J., Woodhouse, M. T., Whale, T. F., Baustian, K. J., Carslaw, K. S., Dobbie, S., O'Sullivan, D. and Malkin, T. L.: The importance of feldspar for ice nucleation by mineral dust in mixed-phase clouds, Nature, 498(7454), 355–358, doi:10.1038/nature12278, 2013.

Augustin-Bauditz, S., Wex, H., Denjean, C., Hartmann, S., Schneider, J., Schmidt, S., Ebert, M. and Stratmann, F.: Laboratory-generated mixtures of mineral dust particles with biological substances: characterization of the particle mixing state and immersion freezing behavior, Atmos. Chem. Phys., 16(9), 5531–5543, doi:10.5194/acp-16-5531-2016, 2016.

Bühl, J., Ansmann, A., Seifert, P., Baars, H. and Engelmann, R.: Toward a quantitative characterization of heterogeneous ice formation with lidar/radar: Comparison of CALIPSO/CloudSat with ground-based observations, Geophys. Res. Lett., 40(16), 4404–4408, doi:10.1002/grl.50792, 2013.

Cantrell, W. and Heymsfield, A.: Production of Ice in Tropospheric Clouds: A Review, Bull. Am. Meteorol. Soc., 86(6), 795–807, doi:10.1175/BAMS-86-6-795, 2005.

Christner, B. C., Morris, C. E., Foreman, C. M., Cai, R. and Sands, D. C.: Ubiquity of Biological Ice Nucleators in Snowfall, Science (80-.)., 319(5867), 1214–1214, doi:10.1126/science.1149757, 2008.

Creamean, J. M., Suski, K. J., Rosenfeld, D., Cazorla, A., Demott, P. J., Sullivan, R. C., White, A. B., Ralph, F., Minnis, P., Comstock, J. M., Tomlinson, J. M. and Prather, K. A.: Dust and biological aerosols from the Sahara and Asia influence precipitation in the Western U.S., Science (80-.)., doi:10.1126/science.1227279, 2013.

DeMott, P. J. and Prenni, A. J.: New Directions: Need for defining the numbers and sources of biological aerosols acting as ice nuclei, Atmos. Environ., 44(15), 1944–1945, doi:10.1016/j.atmosenv.2010.02.032, 2010.

DeMott, P. J., Prenni, A. J., McMeeking, G. R., Sullivan, R. C., Petters, M. D., Tobo, Y., Niemand, M., Möhler, O., Snider, J. R., Wang, Z. and Kreidenweis, S. M.: Integrating laboratory and field data to quantify the immersion freezing ice nucleation activity of mineral dust particles, Atmos. Chem. Phys., 15(1), 393–409, doi:10.5194/acp-15-393-2015, 2015.

Ervens, B. and Feingold, G.: On the representation of immersion and condensation freezing in cloud models using different nucleation schemes, Atmos. Chem. Phys., 12, 5807–5826, doi:10.5194/acp-12-5807-2012, 2012.

Franc, G. D. and Demott, P. J.: Cloud Activation Characteristics of Airborne Erwinia carotovora Cells, J. Appl. Meteorol., 37(10), 1293–1300 doi: 10.1175/1520-0450(1998)037%3C1293:CACOAE%3E2.0.CO;2, 1998.

Fröhlich-Nowoisky, J., Hill, T. C. J., Pummer, B. G., Yordanova, P., Franc, G. D. and Pöschl, U.: Ice nucleation activity in the widespread soil fungus Mortierella alpina, Biogeosciences, 12(4), 1057–1071,

doi:10.5194/bg-12-1057-2015, 2015.

Hartmann, S., Augustin, S., Clauss, T., Wex, H., Šantl-Temkiv, T., Voigtländer, J., Niedermeier, D. and Stratmann, F.: Immersion freezing of ice nucleation active protein complexes, Atmos. Chem. Phys., 13(11), 5751–5766, doi:10.5194/acp-13-5751-2013, 2013.

Hiranuma, N., Augustin-Bauditz, S., Bingemer, H., Budke, C., Curtius, J., Danielczok, A., Diehl, K., Dreischmeier, K., Ebert, M., Frank, F., Hoffmann, N., Kandler, K., Kiselev, A., Koop, T., Leisner, T., Möhler, O., Nillius, B., Peckhaus, A., Rose, D., Weinbruch, S., Wex, H., Boose, Y., DeMott, P. J., Hader, J. D., Hill, T. C. J., Kanji, Z. A., Kulkarni, G., Levin, E. J. T., McCluskey, C. S., Murakami, M., Murray, B. J., Niedermeier, D., Petters, M. D., O'Sullivan, D., Saito, A., Schill, G. P., Tajiri, T., Tolbert, M. A., Welti, A., Whale, T. F., Wright, T. P. and Yamashita, K.: A comprehensive laboratory study on the immersion freezing behavior of illite NX particles: a comparison of 17 ice nucleation measurement techniques, Atmos. Chem. Phys., 15(5), 2489–2518, doi:10.5194/acp-15-2489-2015, 2015a.

Hiranuma, N., Möhler, O., Yamashita, K., Tajiri, T., Saito, A., Kiselev, A., Hoffmann, N., Hoose, C., Jantsch, E., Koop, T. and Murakami, M.: Ice nucleation by cellulose and its potential contribution to ice formation in clouds, Nat. Geosci., 8(4), 273–277, doi:10.1038/ngeo2374, 2015b.

Hoose, C., Lohmann, U., Erdin, R. and Tegen, I.: The global influence of dust mineralogical composition on heterogeneous ice nucleation in mixed-phase clouds, Environ. Res. Lett., 3(2), 25003, doi:10.1088/1748-9326/3/2/025003, 2008.

Kamphus, M., Ettner-Mahl, M., Klimach, T., Drewnick, F., Keller, L., Cziczo, D. J., Mertes, S., Borrmann, S. and Curtius, J.: Chemical composition of ambient aerosol, ice residues and cloud droplet residues in mixed-phase clouds: single particle analysis during the Cloud and Aerosol Characterization Experiment (CLACE 6), Atmos. Chem. Phys., 10(16), 8077–8095, doi:10.5194/acp-10-8077-2010, 2010.

Möhler, O., DeMott, P. J., Vali, G. and Levin, Z.: Microbiology and atmospheric processes: the role of biological particles in cloud physics, Biogeosciences Discuss., 4(4), 2559–2591, doi:hal-00297909, 2007.

Morris, C. E., Georgakopoulos, D. G. and Sands, D. C.: Ice nucleation active bacteria and their potential role in precipitation, J. Phys. IV, 121, 87–103, doi:10.1051/jp4:2004121004, 2004.

Murray, B. J., O'Sullivan, D., Atkinson, J. D. and Webb, M. E.: Ice nucleation by particles immersed in supercooled cloud droplets, Chem. Soc. Rev., 41(19), 6519, doi:10.1039/c2cs35200a, 2012.

Niedermeier, D., Shaw, R. a., Hartmann, S., Wex, H., Clauss, T., Voigtländer, J. and Stratmann, F.: Heterogeneous ice nucleation: exploring the transition from stochastic to singular freezing behavior, Atmos. Chem. Phys., 11(16), 8767–8775, doi:10.5194/acp-11-8767-2011, 2011.

O'Sullivan, D., Murray, B. J., Ross, J. F., Whale, T. F., Price, H. C., Atkinson, J. D., Umo, N. S. and Webb, M. E.: The relevance of nanoscale biological fragments for ice nucleation in clouds, Sci. Rep., 5, 8082, doi:10.1038/srep08082, 2015.

O'Sullivan, D., Murray, B. J., Ross, J. F. and Webb, M. E.: The adsorption of fungal ice-nucleating proteins on mineral dusts : a terrestrial reservoir of atmospheric ice-nucleating particles, Atmos. Chem. Phys., 16, 7879–7887, doi:10.5194/acp-16-7879-2016, 2016.

Petters, M. D. and Wright, T. P.: Revisiting ice nucleation from precipitation samples, Geophys. Res. Lett., 42(20), 8758–8766, doi:10.1002/2015GL065733, 2015.

Polen, M., Lawlis, E. and Sullivan, R. C.: The unstable ice nucleation properties of Snomax(R) bacterial particles, J. Geophys. Res. - Atmos., 121, 11,666–11,678, doi:10.1002/ 2016JD025251, 2016.

Prather, K. a, Bertram, T. H., Grassian, V. H., Deane, G. B., Stokes, M. D., Demott, P. J., Aluwihare, L. I., Palenik, B. P., Azam, F., Seinfeld, J. H., Moffet, R. C., Molina, M. J., Cappa, C. D., Geiger, F. M., Roberts, G. C., Russell, L. M., Ault, A. P., Baltrusaitis, J., Collins, D. B., Corrigan, C. E., Cuadra-Rodriguez, L. a, Ebben, C. J., Forestieri, S. D., Guasco, T. L., Hersey, S. P., Kim, M. J., Lambert, W. F., Modini, R. L., Mui, W., Pedler, B. E., Ruppel, M. J., Ryder, O. S., Schoepp, N. G., Sullivan, R. C. and Zhao, D.: Bringing the ocean into the laboratory to probe the chemical complexity of sea spray aerosol., Proc. Natl. Acad. Sci. U. S. A., 110(19), 7550–5, doi:10.1073/pnas.1300262110, 2013.

Pratt, K. a., DeMott, P. J., French, J. R., Wang, Z., Westphal, D. L., Heymsfield, A. J., Twohy, C. H., Prenni, A. J. and Prather, K. a.: In situ detection of biological particles in cloud ice-crystals, Nat. Geosci., 2(6), 398–401, doi: 10.1038/ngeo521, 2009.

Schnell, R. C. and Vali, G.: Biogenic Ice Nuclei: Part I. Terrestrial and Marine Sources, J. Atmos. Sci., 33(8), 1554–1564, doi:10.1175/1520-0469(1976)033<1554:BINPIT>2.0.CO;2, 1976.

Turner, M. A., Arellano, F. and Kozloff, L. M.: Three separate classes of bacterial ice nucleation structures, J. Bacteriol., 172(5), 2521–2526, doi:PMC208892, 1990.

Vali, G.: Freezing Nucleus Content of Hail and Rain in Alberta, J. Appl. Meteorol., 10(1), 73–78, doi:10.1175/1520-0450(1971)010<0073:FNCOHA>2.0.CO;2, 1971.

Vali, G.: Ice nucleation—A review. Nucleation and Atmospheric Aerosols, M. Kulmala and P. Wagner, Eds., Pergamon, 271–279, 1996.

Vali, G.: Interpretation of freezing nucleation experiments: Singular and stochastic; Sites and surfaces, Atmos. Chem. Phys., 14(11), 5271–5294, 2014.

Welti, A., Lüönd, F., Kanji, Z. A., Stetzer, O. and Lohmann, U.: Time dependence of immersion freezing: an experimental study on size selected kaolinite particles, Atmos. Chem. Phys., 12(20), 9893–9907, doi:10.5194/acp-12-9893-2012, 2012.

Wex, H., Augustin-Bauditz, S., Boose, Y., Budke, C., Curtius, J., Diehl, K., Dreyer, a., Frank, F., Hartmann, S., Hiranuma, N., Jantsch, E., Kanji, Z. a., Kiselev, a., Koop, T., Möhler, O., Niedermeier, D., Nillius, B., Rösch, M., Rose, D., Schmidt, C., Steinke, I. and Stratmann, F.: Intercomparing different devices for the investigation of ice nucleating particles using Snomax® as test substance, Atmos. Chem. Phys., 15(3), 1463–1485, doi:10.5194/acp-15-1463-2015, 2015.

Wolber, P. K., Deininger, C. A., Southworth, M. W., Vandekerckhove, J., van Montagu, M. and Warren, G. J.: Identification and purification of a bacterial ice-nucleation protein., Proc. Natl. Acad. Sci., 83(19), 7256–7260, doi:10.1073/pnas.83.19.7256, 1986.

Wright, T. P. and Petters, M. D.: The role of time in heterogeneous freezing nucleation, J. Geophys. Res. Atmos., 118(9), 3731–3743, doi: 10.1002/jgrd.50365, 2013.

Yankofsky, S. a., Levin, Z., Bertold, T. and Sandlerman, N.: Some Basic Characteristics of Bacterial Freezing Nuclei, J. Appl. Meteorol., 20(9), 1013–1019, doi:10.1175/1520-0450(1981)020<1013:SBCOBF>2.0.CO;2, 1981.

Zobrist, B., Koop, T., Luo, B. P., Marcolli, C. and Peter, T.: Heterogeneous ice nucleation rate coefficient of water droplets coated by a nonadecanol monolayer, J. Phys. Chem. C, 111(1), 2149–2155, doi:10.1021/jp066080w, 2007.